2 MINERνA Physics Goals and Detector Design Drivers

2.8 Nuclear Effects in Neutrino Scattering

2.8.1 Introduction

Most neutrino experiments, including neutrino oscillation experiments, require massive nuclear targets/detectors to obtain useful reaction rates. Analysis of neutrino reactions with nuclear media requires understanding the nuclear environment's effect on the process [1]. There are two general categories of such nuclear effects:

- The neutrino interaction probability on nuclei is modified relative to free nucleons. Nuclear effects of this type have been extensively studied using muon and electron beams, but have not been explored with neutrinos. Depending on the kinematic region, these nuclear effects can be quite different for neutrinos [2], and are important for neutrino energies typical of oscillation experiments.

- Hadrons produced in a nuclear target may undergo final-state interactions (FSI), including rescattering and absorption. These effects may significantly alter the observed final-state configuration and measured energy [3, 4], and are sizable at neutrino energies typical of current and planned neutrino oscillation experiments [41].

The hadron shower observed in neutrino experiments is actually the *convolution* of these two effects. FSI effects are dependent on the specific final states that, even for free protons, differ for neutrino and charged-lepton reactions. The suppression or enhancement of particular final states by nuclear effects also differs for neutrino and charged lepton reactions. For these reasons, measurements of nuclear effects with charged leptons cannot be applied to neutrino-nucleus interactions without considerable care.

To study these questions in MINERνA, carbon, iron and lead targets will be installed upstream of the pure scintillator active detector. To measure the overall effect of the nucleus, the observed interaction rate, hadron spectrum and multiplicity will be measured for all three targets.

2.8.2 Modified Interaction Probabilities

Pronounced nuclear effects have been measured in *charged-lepton* scattering from a number of nuclear targets. The experimental situation is discussed in review papers [6, 7].

The mechanisms of nuclear scattering have also been studied theoretically. These mechanisms appear to be different for small and large Bjorken x as viewed from the laboratory system. Bjorken x is defined as $x = Q^2/2M\nu$, where ν and $\boldsymbol{q}$ are energy and three-momentum transfer to the target and $Q^2 = \boldsymbol{q}^2 - \nu^2$. The physical quantity discriminating between large and small x regions is a characteristic scattering time, which is also known as Ioffe time (or length) $\bar{\tau_I} = \nu/Q^2$ [8]. If τ_I is smaller than the average nuclear separation between nucleons, the process can be viewed as incoherent scattering off bound nucleons. This occurs for larger $x(> 0.2)$.

At small Bjorken x the space-time picture is different. The underlying physical mechanism in the laboratory reference frame can be sketched as a two-stage process. In the first stage, the virtual photon γ^* (or W^* or Z^* for neutrino interactions) fluctuates into a quark-antiquark (or hadronic) state. This

hadronic state then interacts with the target. The uncertainty principle allows an estimate of the average lifetime of such a fluctuation as

$$\tau = 2\nu/(m^2 + Q^2), \tag{1}$$

where m is the invariant mass of the hadrons into which the virtual boson converts. The same scale τ also determines the characteristic longitudinal distances involved in the process. At small x, τ exceeds the average distance between bound nucleons and coherent multiple interactions of this hadronic fluctuation in a nucleus are important. It is well known that the nuclear shadowing effect for structure functions results from coherent nuclear interactions by hadronic fluctuations of virtual intermediate bosons (for a recent review of nuclear shadowing see, e.g., [7]).

Nuclear effects in the incoherent regime at large x If x is large enough to neglect coherent nuclear shadowing, lepton scattering off a nucleus can be approximated as incoherent scattering from bound protons and neutrons. The most pronounced nuclear effects in this region are due to Fermi-motion, nuclear binding [9, 10, 11, 12, 13, 14, 15], and off-shell modification of nucleon structure functions [14, 15, 16, 17, 20].

A widely used approximation in description of nuclear structure functions is to neglect the final state interactions of resulting hadrons with the recoiling nucleus. In this approximation the nuclear structure functions can be written as the bound nucleon structure function averaged (convoluted) with the nuclear spectral function (for derivation and more details see [11, 14, 20]). Since bound nucleons are off-shell particles their quark distributions generally depend on nucleon virtuality k^2 as an additional variable. Off-shell effects in structure functions can be viewed as a way to describe in-medium modification of structure functions. This effect was discussed in terms of different approaches in the literature [13, 17, 14, 16, 19, 20].

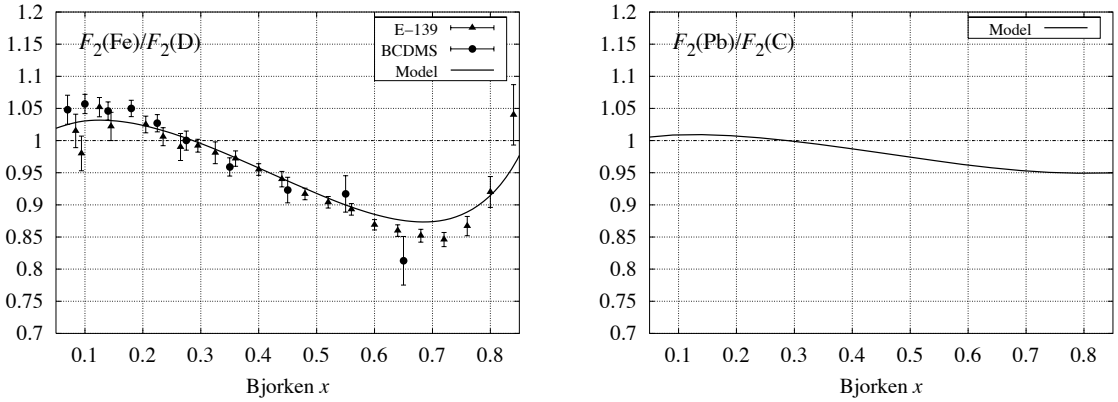

Figure 1: The ratio of iron to deuterium structure functions as measured by SLAC E-139 and CERN BCDMS collaborations in experiments with electron and muon beams (left panel). Also shown are the results of model calculation at fixed $Q^2 = 10\ \mathrm{GeV}^2$ which account for binding, Fermi-motion and off-shell effects in nuclear deep-inelastic scattering [20]. The ratio of lead and carbon structure functions calculated at fixed $Q^2 = 10\ \mathrm{GeV}^2$ within the same approach is presented in the right panel.

Predictions of the convolution approach are compared to data on charged-lepton deep-inelastic scattering in Figure 1. Model calculations of nuclear structure functions use realistic nuclear spectral functions. Data seem to indicate that some off-shell modification of bound nucleon structure function is necessary [20]. The right panel of Figure 1 displays the ratio of lead and carbon structure functions calculated within the same approach. It appears nuclear effects at large x are practically saturated in carbon. Similar effects are predicted for neutrino structure functions F_2 and xF_3. MINERνA will provide valuable information on nuclear effects in this region.

Nuclear effects at small x Nuclear shadowing effects have been discussed extensively in the literature. A recent paper [7] reviews both experimental data and theoretical models of nuclear shadowing for charged-lepton scattering. This effect is interpreted as the coherent interaction of a hadronic component of the virtual photons with the target nucleus. The structure functions at small x can be represented as a superposition of contributions from different hadronic states.

In fixed-target experiments events with small Bjorken x are correlated with low four-momentum transfer (Q^2). At low Q^2 the vector meson dominance model (VMD) appears to be a good tool to study nuclear corrections to structure functions [7, 21]. In VMD the structure functions are saturated by contributions from a few low-mass vector meson states. For the interactions driven by the electromagnetic current usually only the isovector ρ and the isoscalar ω and ϕ mesons are important at low $Q^2 < 1\ \mathrm{GeV}^2$ [21]. The structure functions in this model have strong Q^2 dependence. In the generalized versions of VMD, higher-mass states including the continuum have also been considered, making the model applicable at higher Q^2 [7, 21].

The VMD approach has also been applied to weak interactions [22]. The vector current, in close analogy with the electromagnetic current, is assumed to be saturated by ρ meson contribution at low Q^2. The axial-vector channel requires inclusion of contributions from the axial-vector meson a_1. There are still a number of interesting physics questions related to the analysis of the axial-vector channel for neutrino interactions.

It should be emphasized that neutrino scattering at low Q^2 is dominated by the axial current. Indeed, contributions to the structure functions (and cross-sections) from the vector current vanish as $Q^2 \to 0$ due to vector-current conservation. The axial current is not conserved and for this reason the longitudinal structure function F_L does not vanish at low Q^2. It was observed long ago by Adler that neutrino cross-sections at low Q^2 are dominated by the contribution from the divergence of the axial current [23]. The latter, because of PCAC, is saturated by the pion contribution, so low Q^2 neutrino cross-sections and structure functions are determined by pion cross-sections. For the longitudinal structure function at low Q^2 the Adler relation is

$$2xF_L^{\mathrm{PCAC}} = \frac{f_\pi^2}{\pi}\sigma_\pi(s, Q^2), \tag{2}$$

where $f_\pi = 0.93 m_\pi$ is the pion decay constant (m_π is the pion mass) and $\sigma_\pi(s, Q^2)$ the total pion cross-section at the center-of-mass energy $s = Q^2(1/x - 1) + M^2$ for an off-shell pion with mass $\sqrt{Q^2}$. Equation (2) determines the dominant contribution to F_2 and neutrino cross-sections at small Q^2 for nucleon and nuclear targets.

It is important to realize that Eq. (2) is not a consequence of the pion dominance of the axial current, i.e. fluctuation of the axial current to a pion which interacts with the target [26]. Indeed, the single-pion fluctuation of the axial current gives a vanishing contribution to the neutrino cross-section. Instead, the axial current in neutrino interactions can produce heavy states such as the a_1 meson and $\rho\pi$ pair, which

interact with the target. The overall contribution of all such states is described by the PCAC relation. The detailed mechanism of this phenomenon is not fully understood and MINERνA can provide new insights on physics driven by the axial current in neutrino interactions.

The strength of nuclear shadowing is controlled by mesonic cross-sections σ_v for the vector current. In the axial-vector channel the relevant quantity is the pion cross-section. To quantitatively understand nuclear effects, the multiple scattering effect on the cross-section is calculated using Glauber–Gribov multiple scattering theory [24, 25, 21, 26]. If l_f is small compared with the nuclear radius, as is the case for heavy nuclei, then multiple scattering effects are important. It should be emphasized that the multiple scattering correction is negative because destructive interference of the forward scattering amplitudes on the upstream nucleons causes *shadowing* of virtual hadron interactions on the back-face nucleons.

The onset of coherent nuclear effects can be estimated by comparing the coherence length of hadronic fluctuation L_c with the average distance between bound nucleons in the nucleus d. For hadronic fluctuation of the vector current L_c is similar to the fluctuation time τ from Eq. (1), where m is the mass of hadronic state in question. Coherent nuclear effects occur if the fluctuation time is large enough $\tau > d$. This condition requires high energy transfer ν and, as is clear from Eq. (1), the coherent region begins at lower energy for smaller masses m. Since $\tau < 2\nu/Q^2$ for any intermediate state, the region of coherent nuclear effects is limited to small x for any Q^2, $x < 1/Md$. Nuclear shadowing saturates if $L_c \gg R$, which happens at small x, and the condition $L_c \sim R$ defines the transition region with strong x dependence of the ratio $\delta\sigma_A/\sigma_N$.

For the axial-vector current, the fluctuation time τ is also given by Eq. (1). However, as argued in [26], the fluctuation and coherence lengths are not the same in this case. In particular, the coherence length is determined by the pion mass m_π in Eq. (1) because of the dominance of off-diagonal transitions like $a_1 N \to \pi N$ in nuclear interactions. Since the pion mass is much smaller than typical masses of intermediate hadronic states for the vector current (m_ρ, m_ω, etc.), the coherence length L_c of intermediate states of the axial current at low Q^2 will be much larger than L_c for the vector current. A direct consequence of this observation is early onset of nuclear shadowing in neutrino scattering at lower energy and Q^2 compared to charged-lepton scattering.

Figure 2 shows the calculated ratios of iron to nucleon and lead to carbon structure functions at two different Q^2 values as a function of x. We also compare the nuclear shadowing effect for muon and neutrino scattering. The basic reason for the earlier onset of nuclear shadowing in neutrino scattering and different behavior in the transition region is the difference in correlation lengths of hadronic fluctuations between the vector and axial-vector currents. This is also illustrated by the observation that for a given Q^2 the cross-section suppression due to shadowing occurs for much lower energy transfer (ν) in neutrino interactions than for charged leptons.

The relative nuclear shadowing effect for the structure function xF_3 should be substantially different than that of F_2 [27]. This is because xF_3 describes the correlation between the vector and the axial-vector current in neutrino scattering. In terms of helicity cross-sections, xF_3 is given by the cross-section asymmetry between the left- and right-polarized states of the virtual W boson. It is known that such a difference of cross-sections is strongly affected by Glauber multiple scattering corrections in nuclei. This leads to enhanced nuclear shadowing of xF_3.

The resulting ratio of lead and carbon structure functions are shown in Figure 3. Unlike nuclear effects at large Bjorken x (Figure 1), there are substantial, structure-function dependent nuclear effects at small x. MINERνA can provide a unique tool to study these effects.

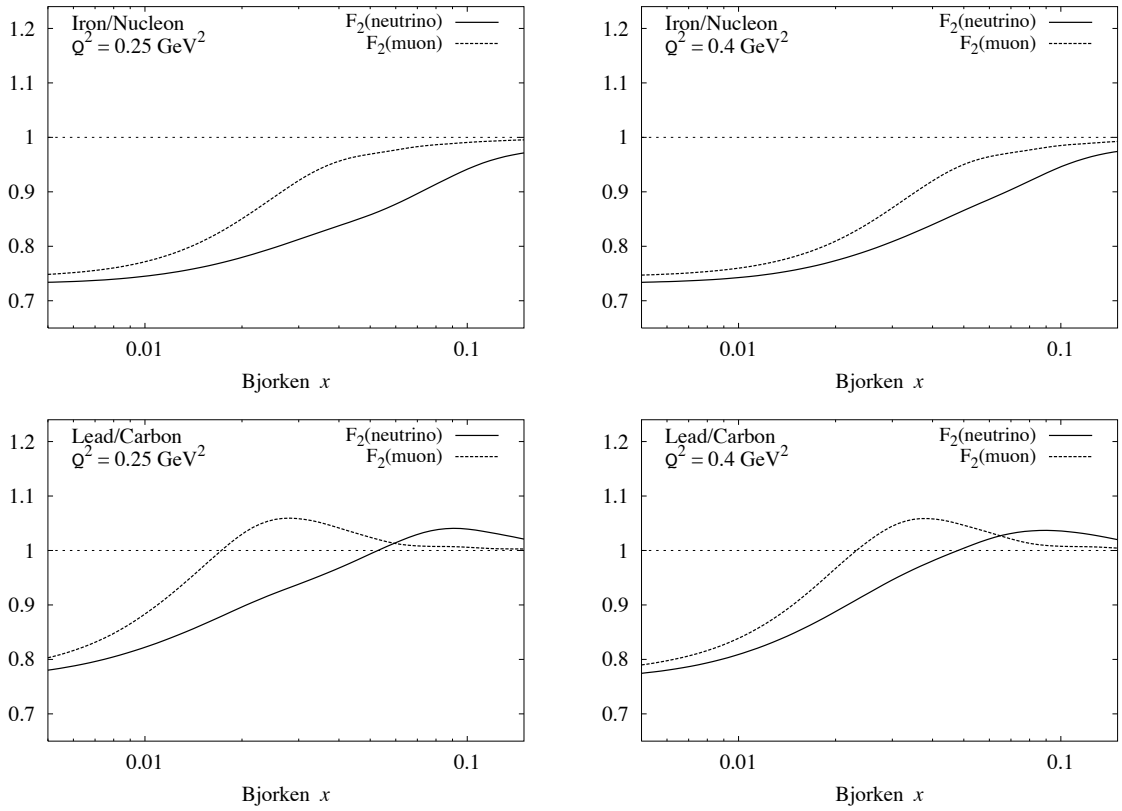

Figure 2: The ratio of iron to nucleon (upper row) and lead to carbon neutrino CC structure functions F_2^ν calculated at two different Q^2 within an approach based on PCAC and VMD (solid line). The dashed line shows similar ratios for the muon structure function F_2^μ.

Determination of $\sin^2\theta_W$ The rates of neutral-current (anti-)neutrino scattering are directly determined by $\sin^2\theta_W$. Therefore the measurement of NC/CC ratios of neutrino cross-sections provides a valuable tool for determination of $\sin^2\theta_W$. For an isoscalar target (e.g. the isoscalar combination of proton and neutron, or for deuterium) a relation between neutrino–antineutrino asymmetries in the NC and CC DIS cross-sections was derived by Paschos and Wolfenstein [28]

$$R^- = \frac{\sigma^\nu_{\rm NC} - \sigma^{\bar\nu}_{\rm NC}}{\sigma^\nu_{\rm CC} - \sigma^{\bar\nu}_{\rm CC}} = \frac{1}{2} - \sin^2\theta_W, \tag{3}$$

where θ_W is the weak mixing angle. A similar relation also holds for the NC/CC ratio of structure functions

$$F_3^{\rm NC}(x,Q^2)/F_3^{\rm CC}(x,Q^2) = 1 - 2\sin^2\theta_W, \tag{4}$$

where $F_3^{\rm CC}$ is the neutrino and antineutrino averaged structure function, $F_3^{\rm CC} = (F_3^\nu + F_3^{\bar\nu})$.

If only the contributions of light quarks are taken into account, the PW relationship is a direct result of isospin symmetry. This ensures that various strong interaction effects, including nuclear effects,

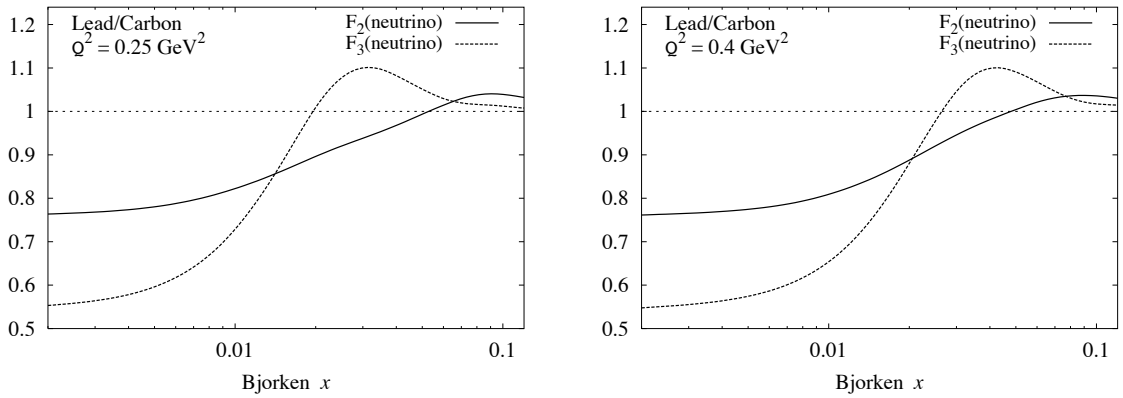

Figure 3: The ratio of lead to carbon neutrino charged-current structure functions F_2 calculated in an approach based on PCAC and VMD at two different Q^2 (solid line). The corresponding ratio for xF_3 is shown by the dashed curve.

cancel out in R^- for an isoscalar target, making Eq. (3) a powerful tool for measurement of the mixing angle in neutrino scattering.

The targets used in neutrino experiments are usually heavy nuclei, such as iron in the NuTeV experiment [29]. Heavy nuclei typically have an excess of neutrons over protons and therefore are not isoscalar targets. For a non-isoscalar target the relations (3) and (4) are violated by contributions from isovector components of nuclear parton distribution functions. Nuclear corrections to relations (3) and (4) were recently studied in [30, 31, 32], which showed that nuclear effects enter through non-isoscalar effects in the target. These studies suggest that nuclear corrections should be greatly reduced for isoscalar targets like carbon. MINERνA, with its lead, iron, and carbon targets, can directly measure the NC/CC ratio for several nuclear targets to explore these effects experimentally.

2.8.3 Final-state Interactions

Overview Interactions of few-GeV neutrinos with nuclei often produce resonances which decay to pions. Any attempt to reconstruct the incident neutrino energy based on the total observed energy must account for pion interactions within the target nucleus. Existing neutrino interaction Monte Carlos (such as INTRANUKE [33]) handle intra-nuclear pion interactions crudely and have generally not incorporated the latest knowledge of pion interactions.

The concern is mainly with pions in the 100–500 MeV range, where the interaction cross-sections are highest. In this range the pion/nucleon cross-section is dominated by the strong $\Delta(1232)$ resonance. The Δ is a fairly narrow (about 100 MeV) resonance, and the pion-nucleon cross-section reflects this, with a peak near 200 MeV pion energy which drops quickly above and below this. The pion/nucleus cross-section exhibits a similar behavior, with a less pronounced drop-off at higher energy. The charged-pion/nucleus cross-section has four important components in the intermediate energy range: elastic scattering (nucleus left in the ground state), inelastic scattering (nucleus left in an excited state or nucleon knocked out), true absorption (no pion in the final state), and single charge exchange (neutral pion in the final state).

Neutrino detectors are mainly iron (absorber), oxygen (water) and carbon (scintillator). The total pion–carbon cross-section is 600 mb, with elastic and inelastic cross-sections about 200 mb each, and absorption about 160 mb. The total pion-iron cross-section is about 1700 mb, with elastic and absorption about 600 mb each, and inelastic about 400 mb. Cross-sections for positive and negative pions are nearly the same because nuclei contain about the same number of protons and neutrons. These very large cross-sections mean that many pions will undergo some nuclear reaction within the target nucleus. In elastic and most inelastic reactions the scattered pion will not, because of its small mass, lose much energy. However, absorbed pions will lose all of their kinetic and mass energy. Of the four components of this intra-nuclear cross-section, the absorption probability within the interaction nucleus is roughly 30%. Figure 4 [42] shows absorption cross-sections for various nuclei as a function of pion energy.

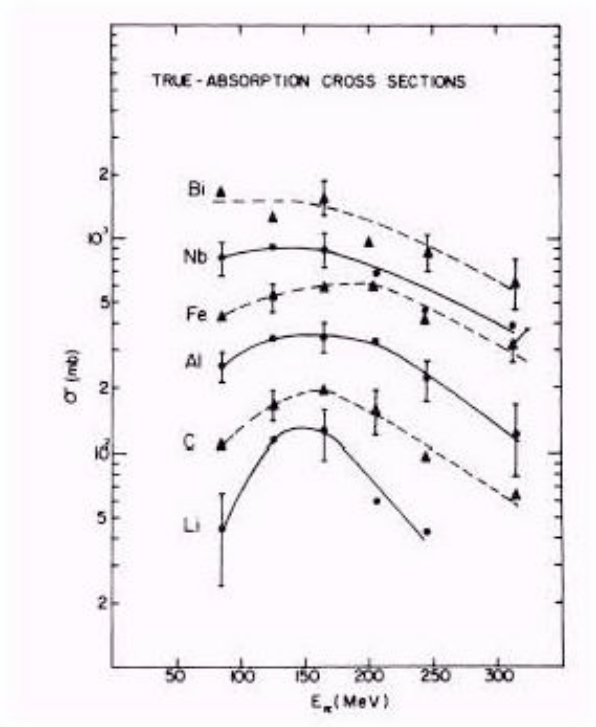

Figure 4: The absorption cross-sections for various nuclei as a function of pion energy.

Pion absorption cannot occur on a single nucleon due to energy and momentum conservation. The simplest absorption mechanism is on two nucleons. Because absorption appears to proceed mainly through $N-\Delta$ intermediate states, an isospin zero (np) pair is the primary candidate. Such an absorption for a positive pion would give two energetic protons whose kinetic energy nearly equaled the total pion energy. However, early studies of pion absorption found this was not the most probable mechanism.

In the 1990's two large solid angle detectors, the LAMPF BGO Ball and the PSI LADS detector, were built to study pion absorption. The somewhat surprising result from both experiments was that pion absorption is dominated by three body absorption [34]. For positive pions, the absorption on a pnn triplet (leading to a ppn final state) was the most common. This was observed even in ^{4}He. The absorption in heavier nuclei also appears to proceed mainly through a three-body mechanism, although increased initial state interactions (pion re-scattering) and final-state interactions (nucleon re-

scattering) result in four to five nucleons being emitted. Typically the final-state contains more neutrons than protons. The absorption process, which is still not well understood theoretically, largely fills the available phase space thus giving a wide range of nucleon energies with little angular dependence. Because much of the energy is in neutrons, the visible energy is well below the total pion energy. Even in carbon more than half the energy is lost to unobserved particles, a fraction which increases with pion energy and with A [35].

The situation is worse for negative pions. Charge symmetry would indicate that the primary absorption should be on a ppn triplet leading to a pnn final state. In this case, most of the pion energy would be in neutrons, and hence effectively invisible. However, if the interaction vertex and one proton energy is known, and the angles of the outgoing neutrons are known, the total energy of the three nucleons can be estimated. Monte Carlo studies with realistic absorption models will be needed to determine the accuracies of such estimates.

Although neutral pions escaping the nucleus will decay, usually to two photons, the mean distance traveled before decay is a few nanometers, much greater than the size of the nucleus. Thus the absorption of neutral pions in the interaction nucleus must also be accounted for in any study of resonance production.

For MINERνA, studies with INTRANUKE have begun to explore the sensitivity to the probability of pion absorption in the interaction nucleus. Monte Carlo routines are being modified to treat pion absorption more realistically. Unfortunately there are essentially no measurements of pion absorption above 500 MeV. The fine spatial resolution and 4π acceptance of MINERνA will allow study of these interactions, especially in carbon.

Nuclear transparency A second nuclear interaction process which affects the observed energy is final state interaction of a nucleon in the struck nucleus. An outgoing nucleon has a substantial probability of interacting in the nucleus. These probabilities have been measured, most recently at Jefferson Lab, with some precision. The experiments used $(e, e'p)$ coincidence reactions, and the cross-section for finding the scattered electron in the quasi-elastic peak was compared to the cross-section for finding the coincident proton.

Unlike pion absorption, there is little available information on what happens to the scattered nucleon. Of course, most either scatter from a single nucleon quasi-elastically or produce a pion (for protons above 600 MeV). Improving Monte Carlo routines to model this interaction should allow us to better estimate the total final state energy. As for pion absorption, the good resolution, neutron detection capability, and full solid angle coverage of MINERνA should allow measurement of the actual final states and help constrain the Monte Carlo models.

2.8.4 Nuclear Effects in MINERνA

To study nuclear effects in MINERνA, carbon, iron and lead targets will be installed upstream of the pure scintillator active detector. The currently preferred configuration involves a total of 9 planes, with each plane divided transversely into C, Fe and Pb wedges. As one proceeds from upstream to downstream, the C, Fe and Pb targets exchange (rotate) positions. A scintillator module of four views (X,U,X,V) separates each of the planes. The total mass is over 1 ton of Fe and Pb and somewhat over 0.5 ton of C. Since the pure-scintillator active detector acts as an additional 3-5 ton carbon target (CH), the pure graphite (C) target is mainly to check for consistency. For the standard four-year run described

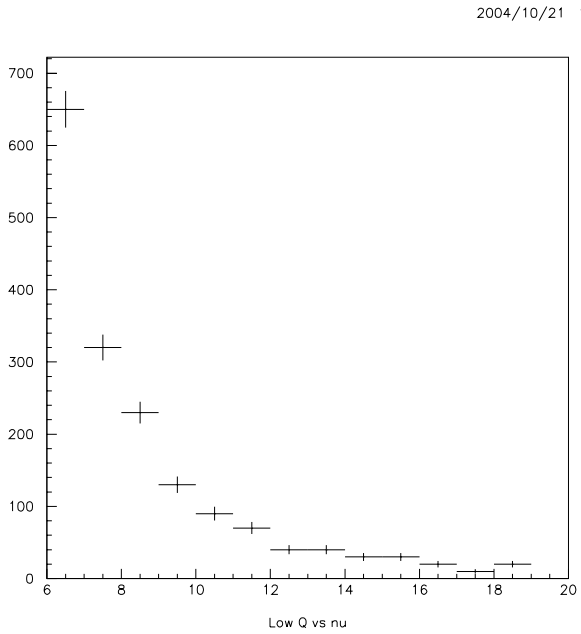

Figure 5: The expected event sample per target with $Q^2 \leq 0.4\text{GeV}^2$ and $\nu \geq 6$ GeV.

in the proposal, MINERνA would collect over 740 K events on Fe and Pb, 430 K events on C as well as 2.3 M events on the scintillator in the fiducial volume.

Measuring modified interaction probabilities To measure this nuclear effect, the cross-section and resulting structure functions $F_2(x,Q^2)$ and $xF_3(x,Q^2)$ will be measured for the three target nuclei of C, Fe and Pb. For the standard 4-year run we expect around 740 K events per target distributed in x depending on the W-region in question. For an A-dependent comparison in the DIS region ($W \geq 2$ GeV and $Q^2 \geq 1$ (GeV/c)^2) we would have 330 K events per target with 66 K events per target in the shadowing region ($x \leq 0.1$) and 20 K events per target in the high-x region ($x \geq 0.5$).

To study the axial-vector nuclear shadowing effects expected at low Q^2 (non-DIS events) and low ν we will have 133 K events per target with $Q^2 \leq 1.0$ (GeV/c)^2 and $x \leq 0.1$. For example, the expected distribution of events with $Q^2 \leq 0.4$ (GeV/c)^2 and $\nu \geq 6$ GeV (the region where the largest differences from charged-lepton shadowing are expected) is shown in Figure 5. With these samples, MINERνA can measure the expected difference in lead to carbon shadowing for charged leptons compared to neutrinos to just under three standard deviations (statistical).

Measuring final state interactions The NEUGEN Monte Carlo has been used to study MINERνA's sensitivity to nuclear effects. Nuclear effects in NEUGEN are controlled by the INTRANUKE processor. This processor incorporates a probability for pion absorption based on earlier electroproduction absorption studies and lower-statistics Ne/H_2 neutrino bubble chamber data. The observed phenomenon of hadron formation length, which increases the transparency and reduces final-state interactions, is incorporated. The particular model used for pion absorption, which is currently being improved and updated, assumes that absorption eliminates a pion and the resulting nucleons are themselves either absorbed in the nucleus or are too low in energy to be observed.

To determine MINERνA's sensitivity to the predictions of this model, the assumed probability for

pion absorption in INTRANUKE has been increased by three standard deviations and then decreased by the same amount, which essentially turns off pion absorption completely. The multiplicity and a simple, crude estimate of the visible hadron energy have been examined under these extreme conditions. Other nuclear effects such as intra-nuclear scattering and hadron formation length have not been altered from their nominal values. Figure 6 shows both the true and reconstructed multiplicity distributions for carbon. Unfortunately, the available tracking software fails to reconstruct many of the tracks. We expect this problem to be resolved when full pattern recognition and a more robust tracker become available. For the present study, we will use the true multiplicities.

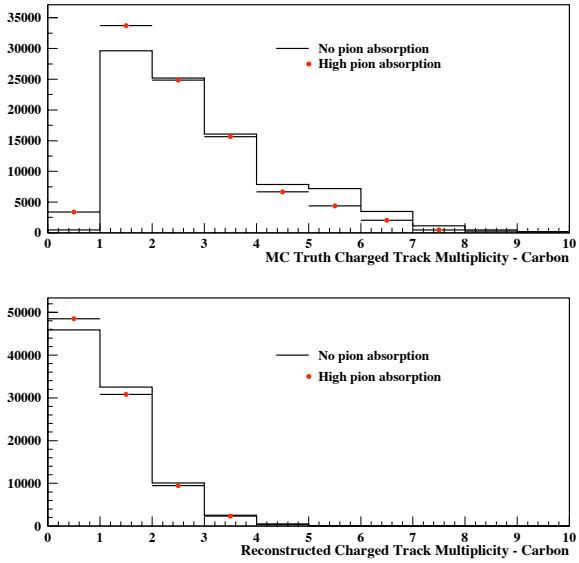

Figure 6: The shift in the true and reconstructed multiplicity distributions between the two values assumed for pion absorption on carbon described in the text.

The next series of figures show the predicted "asymmetry" of the true multiplicity and visible hadron energy. The asymmetry is defined as the percentage change under these extreme assumptions. That is, the bin contents at plus three standard deviations minus the bin contents at minus three standard deviations, divided by bin contents at minus three standard deviations. Figure 7 shows the asymmetry of the true multiplicity for carbon and iron. There is a dramatic effect for carbon, as the high absorption value increases the number of 0-track events by over a factor of six compared to the no-absorption case. This is because the other nuclear effects, being unchanged, are minimal for carbon. Since intra-nuclear rescattering increases as $A^{1/3}$ and the suppression due to hadron formation length decreases as $A^{1/3}$, non-absorption nuclear effects are minimal for carbon and already sizable for lead. If this model is realistic, the carbon multiplicity distribution should be quite sensitive to the probability of absorption.

Final determination of the visible hadronic energy will be an involved process for this experiment. For now, we use the most primitive estimate of this quantity, an uncorrected version derived from the total light output of the hadron shower. In the real data analysis this can be refined through measurements of stopping/decaying particles. With this crude estimate, the change in hadron energy for iron and lead are shown in Figure 8. There is a significant increase in the number of events with E_H less than 3 GeV and a corresponding decrease in the number of events with higher E_H, as one would expect. MINERνA will collect several times these statistics and should be able to measure this effect at even

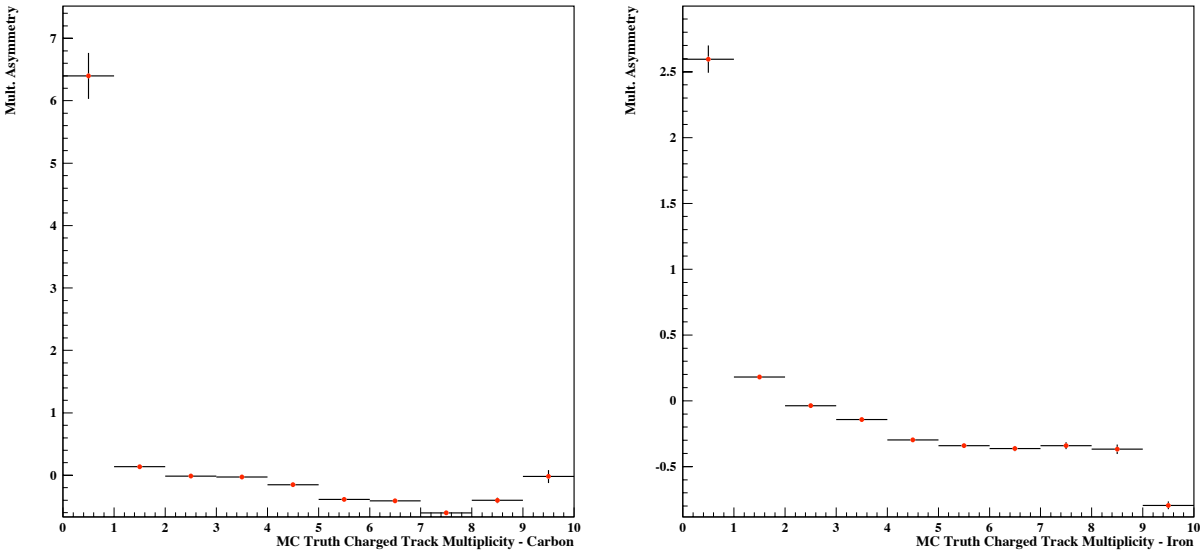

Figure 7: The fractional change in true multiplicity distributions between the two values assumed for pion absorption on carbon (left) and iron (right), as described in the text.

higher hadron energy.

Since the incoming neutrino energy is not known *a priori*, the measured **muon** kinematics will be tested as a basis for comparing the visible hadron shower across nuclear targets to determine whether a nuclear correction-factor can be parameterized as a function of the observed muon angle and energy. The muon is relatively free from nuclear dependent effects and serves well as an A-independent normalization. For example, the quantity:

$$Q' = E_\mu \sin^2(\theta/2) \tag{5}$$

is representative of the 4-momentum transfer to the nucleon or quark (divided by E_ν) and reflects the energy-momentum transferred to the hadronic vertex. The distribution of events in this quantity is peaked toward low Q'. with half the events below $Q' = 1.0$ GeV.

References

[1] D. Drakoulakos *et al.* [Minerva Collaboration], fine-grained detector in the NuMI beam," arXiv:hep-ex/0405002. Pgs. 99 - 108, 192 - 200.

[2] B.Z. Kopeliovich, hep-ph/0409079.

[3] M.K. Jones *et al.*, Phys. Rev. **C48**, 2800 (1993); R.D. Ransome *et al.*, Phys. Rev. **C46**, 273 (1992); R.D. Ransome *et al.*, Phys. Rev. **C45**, R509 (1992).

[4] D. Rowntree *et al.*, Phys. Rev. **C60**, 054610 (1999); B. Kotlinksi *et al.*, Eur. Phys. J. **A9**, 537 (2000).

[5] E. A. Paschos, M. Sakuda, I. Schienbein and J. Y. Yu, arXiv:hep-ph/0408185.

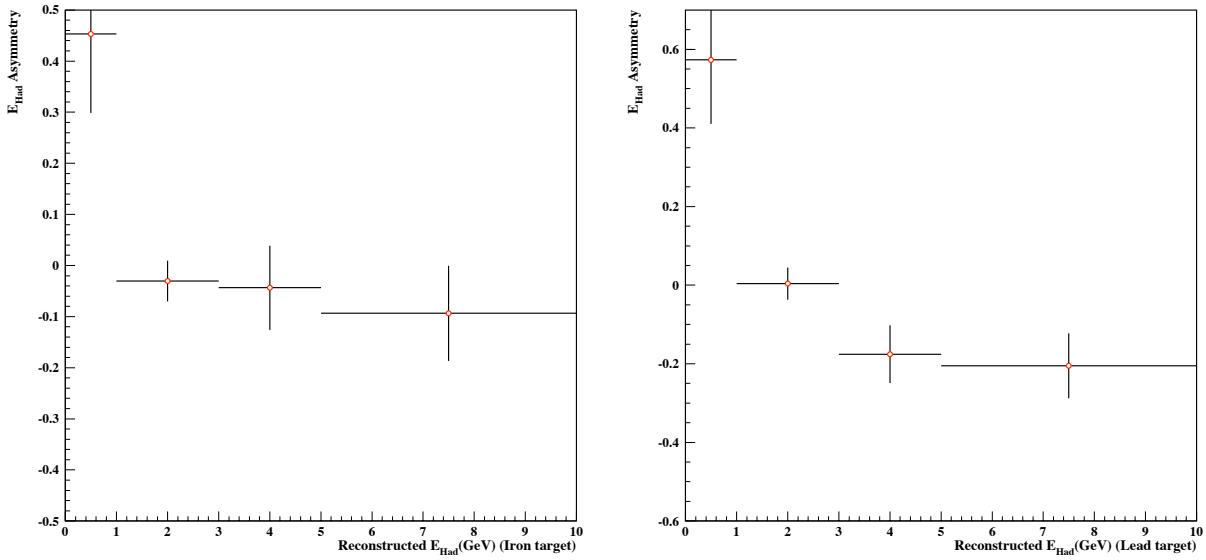

Figure 8: The fractional change in the visible hadron energy distributions between the two values of pion absorption on iron (left) and lead (right), as discussed in the text.

[6] M. Arneodo, Phys. Rept. **240**, 301 (1994).

[7] G. Piller and W. Weise, Phys. Rept. **330**, 1 (2000).

[8] B. L. Ioffe, V. A. Khoze, and L. N. Lipatov, *Hard processes: Phenomenology, Quark-Parton Model* (Elsevier Science Publishers, North Holland, 1984).

[9] G.B. West, Ann. Phys. **74** (1972) 464.

[10] S. V. Akulinichev, S. A. Kulagin, and G. M. Vagradov, Phys. Lett. B **158**, 485 (1985); S. V. Akulinichev, S. Shlomo, S. A. Kulagin, and G. M. Vagradov, Phys. Rev. Lett. **55**, 2239 (1985).

[11] S. A. Kulagin, Nucl. Phys. A **500**, 653 (1989).

[12] C. Ciofi degli Atti and S. Liuti, Phys. Rev. C **41**, 1100 (1990).

[13] F. Gross and S. Liuti, Phys. Rev. C **45**, 1374 (1992).

[14] S. A. Kulagin, G. Piller and W. Weise, Phys. Rev. C **50**, 1154 (1994).

[15] S. A. Kulagin, W. Melnitchouk, G. Piller, and W. Weise, Phys. Rev. C **52**, 932 (1995).

[16] S. A. Kulagin, Nucl. Phys. A **A 640**, 435 (1998).

[17] W. Melnitchouk, A. W. Schreiber and A. W. Thomas, Phys. Rev. D **49**, 1183 (1994).

[18] J. Gomez, *et al.*, Phys. Rev. D **49**, 4348 (1994).

[19] S. I. Alekhin, S. A. Kulagin and S. Liuti, Phys Rev. D **69**, 114009 (2004).

[20] S. A. Kulagin and R. Petti, paper in preparation.

[21] T. H. Bauer, R. D. Spital, D. R. Yennie and F. M. Pipkin, Rev. Mod. Phys. **50**, 261 (1978) [Erratum-ibid. **51**, 407 (1979)].

[22] C. A. Pickety, and L. Stodolsky, Nucl. Phys. B **15**, 571 (1970).

[23] S. L. Adler, Phys. Rev. **135**, B963 (1964).

[24] R. J. Glauber, Phys. Rev. **100**, 242 (1955).

[25] V. N. Gribov, Sov. Phys. JETP **29**, 483 (1970) [Zh. Eksp. Teor. Fiz. **56**, 892 (1969)] ; Sov. Phys. JETP **30**, 709 (1970) [Zh. Eksp. Teor. Fiz. **57**, 1306 (1969)].

[26] B. Z. Kopeliovich, and P. Marage, Int. J. Mod. Phys. A **8**, 1513 (1993).

[27] S. A. Kulagin, arXiv:hep-ph/9812532.

[28] E. A. Paschos and L. Wolfenstein, Phys. Rev. D **7**, 91 (1973).

[29] G. P. Zeller *et al*. [NuTeV Collaboration], Phys. Rev. Lett. **88**, 091802 (2002) [Erratum-ibid. **90**, 239902 (2003)] [arXiv:hep-ex/0110059].

[30] S. A. Kulagin, Phys. Rev. D **67**, 091301 (2003) [arXiv:hep-ph/0301045].

[31] S. A. Kulagin, arXiv:hep-ph/0406220.

[32] S. A. Kulagin, arXiv:hep-ph/0409057.

[33] R. Merenyi *et al*., Phys. Rev. D **45**, 743 (1992), W. A. Mann *et a l*., unpublished.

[34] C.H.Q. Ingram, Nucl. Phys. A **684**, 122 (2001).

[35] M. K. Jones *et al*., Phys. Rev. C **48**, 2800 (1993).

[36] M. Nakahata *et al*, Nucl. Instrum. Meth. **A421**, 113 (19 99); E. Blaufuss *et al*, Nucl. Instrum. Meth. **A458** 638 (2001).

[37] M. Diwan and J. Nelson, NuMI-NOTE-STEEL-0639 (2000)

[38] PhD Thesis of C. Smith, University College London, London, 2002 *Calibration of the MINOS Detectors and Extraction of Neutrino Oscillation Parameters*; PhD Thesis of R. Nichol, University College London, London, 2003 *Calibration of the MINOS Detectors*

[39] PhD thesis of M. A. Kordosky, University of Texas at Austin, August 2004 *Hadronic Interactions in the MINOS Detectors*

[40] PhD thesis of P. L. Vahle, University of Texas at Austin, August 2004 *Electromagnetic Interactions in the MINOS Detectors*

[41] E. A. Paschos, L. Pasquali and J. Y. Yu, Nucl. Phys. B **588**, 263 (2000) and E. A. Paschos, J. Y. Yu and M. Sakuda [arXiv:hep-ph/0308130].

[42] D. Ashery *et al.*, Phys. Rev. **C23**, 2173 (1981).

[43] H. Gallagher, Nucl. Phys. Proc. Suppl. **112**, 188 (2002)

[44] NuMI Fluxes courtesy of Mark Messier

[45] The simulation assumed the active material was resistive plate chambers and the absorber was particle board (hydrocarbons).

[46] G.P.Zeller, submitted to proceedings of 2nd International Workshop on Neutrino - Nucleus Interactions in the Few GeV Region (NUINT 02), Irvine, California, 12-15 Dec 2002 [hep-ex/0312061]

999